Influence of RF Probe Tip Geometry on Surface Wave Generation in Millimeter-Wave on-Wafer Characterization

Arash Masrouri, Quentin Courte, Jean-Pierre Raskin, Dimitri Lederer
ICTEAM, Université catholique de Louvain, Belgium
{arash.masrouri, quentin.courte, jean-pierre.raskin, dimitri.lederer}@uclouvain.be

***Abstract*— This paper investigates the influence of probe tip geometry on the excitation of surface waves and radiated power in high-frequency on-wafer measurements, focusing on two commercially available RF probes with planar and microstrip tip structures. The study is conducted across the DC-110 GHz frequency band and employs two distinct approaches: the first studies surface wave generation at the contact point between the probe and the substrate, while the second examines the surface wave power. For both approaches, simulation and measurement results are presented and aligned with each other, showing that the probe with planar tip configuration contributes more to the generation of surface waves and radiation into the air, compared with the microstrip tip probe.**

***Keywords*— RF probe, surface wave, probes coupling, on-wafer characterization, electromagnetic simulation.**

I. Introduction

The ever-increasing demand for high-speed and bandwidth-intensive applications has evolved the design and fabrication of semiconductor devices significantly, particularly in the millimeter-wave (mmW) and terahertz (THz) frequency ranges. Driven by the rise of advanced applications such as Antenna- on-Chip (AoC), Antenna-in-Package (AiP), radar systems and others, alongside advancements in silicon processes, the need for precise wafer-level characterization has become increasingly crucial [1], [2].

As a key component in characterizing the true performance of a device under test (DUT), RF probes play a vital role in transitioning signals from coplanar waveguide (CPW) lines to the vector network analyzer (VNA). However, on-wafer probing is not without challenges, particularly as measurement frequencies increase, parasitic effects that can impact the accuracy of the measurement become more pronounced. These parasitics arise from various sources, including radiation from probe tips, scattering from the probe body, and interactions between the probe body and the chuck. Previous studies demonstrated that the primary contributor is the interaction between the probe tips and the substrate [3], [4].

Despite adapting various calibration methods, yet there exist limitations in the accuracy of calibration at higher frequencies, where the role of surface-wave excitation, probe geometry and calibration standards is highlighted [5]–[7].

In a measurement setup, boundary conditions from the substrate and chuck determine which surface wave modes can propagate, each with unique propagation characteristics [8].

Additionally, the choice of RF probe significantly affects surface wave excitation, as different probe designs interact with the substrate in distinct ways [4].

The goal of this paper is to investigate how different probe tip geometries contribute to the generation of surface waves through a comparative study of two commercially available RF probes with GSG tip configuration, $100\mu m$ pitch, dedicated to DC-110GHz frequency band. Two approaches are presented, each focusing on distinct aspects of surface wave behavior, with simulation and measurement results discussed for both. The first approach studies surface wave generation at the contact point between the probe and the substrate, while the second examines surface wave power.

II. Model Description And Methodology

Probes are modeled using microscope and x-ray tomography techniques. The entire probe body, including the tips and the body, is incorporated into the simulations. Fig. 1 provides a visualization of the modeled probe tips. Fig. 1a and Fig. 1b display, respectively, the probe with a planar tip and microstrip tip geometry. In the following section, both presented approaches aim to study the excitation of surface waves in the substrate.

Measurements are performed using the MPI TS-200 THz probe system, with a N5227B PNA from Keysight Technologies covering DC-67 GHz range, connected to N5295AX-03 120 GHz frequency extenders from the same vendor. To have consistency between simulations and measurements, a *SOLR* (short-open-load-reflect) calibration is performed using the 85059B, 1mm calibration kit from Keysight Technologies. This calibration shifts the reference planes to the end of the 1 mm RF coaxial cables, which connect the mmW heads to the probes. The calibration substrate used in this study is a 0.254 mm thick commercial alumina substrate from FormFactor [9]. High-Frequency Structure Simulator (HFSS) from ANSYS is used for simulations.

A. Generation And Propagation Of The Surface Wave Mode

To address the fundamental question of surface wave excitation in the calibration substrate, an experiment is conducted using a pair of *THRU*s on the substrate, spaced 3.7 mm apart (Fig. 2a). First, two identical probes are placed in the air at the same 3.7 mm spacing with no substrate beneath,

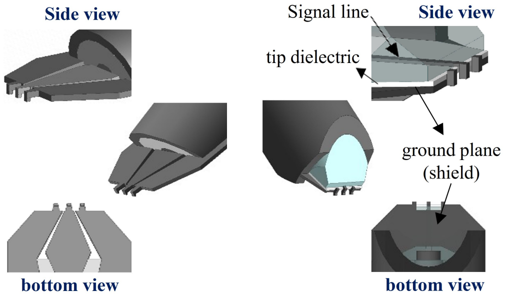

(a) (b)

Fig. 1. Side and bottom view of the studied probe tips: (a) planar tips, (b) microstrip tips.

and the transmission (S_{21}) is recorded. Next, the probes are landed on the *THRU*s: one on the first *THRU* as the surface wave exciter, the other on the second as the receiver (Fig. 2b). This configuration is tested with both a metallic and a ceramic chuck under the alumina substrate.

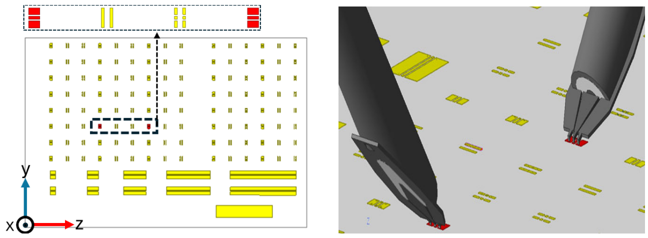

(a) (b)

Fig. 2. (a) map of the calibration substrate; (b) probes in contact with *THRU*s on calibration substrate.

In Fig. 3 simulation and measurement results for two different scenarios of the probes are presented: (1) probes in the air, (2) probes landed on the *THRU*s.

While the probes are in the air, the probe-to-probe coupling is primarily due to radiation from the probe tips, with the planar tip probe generally showing higher coupling across the band. After landing the probes on the *THRU*s with the substrate on a metallic chuck, the coupling (S_{21}) increases significantly, especially beyond 55 GHz, as shown in Fig. 3c and Fig. 3d for both simulation and measurement. This rise in S_{21} is attributed to surface wave excitation within the substrate. Minor discrepancies between simulation and measurement stem from *SOLR* calibration quality, material property uncertainties, dimensional tolerances, and measurement noise.

As discussed in [10], in a grounded dielectric slab, the first surface wave mode is TM_0, which has no cut-off frequency and can propagate at any frequency. The next higher-order mode, TE_1, for an alumina substrate with a thickness of 0.254 mm, has a cut-off frequency of 99 GHz.

To further analyze the rise in S_{21}, three specific frequencies are selected: 40 GHz, where no strong coupling is yet observed; 80 GHz, where the coupling has already risen significantly for the metallic chuck; and 110 GHz, the high-end of the frequency band, where the TE_1 mode for grounded dielectric slab is also excited. The electric field vector in the substrate below the probe tips is plotted for metallic chuck configuration as illustrated in Fig. 4.

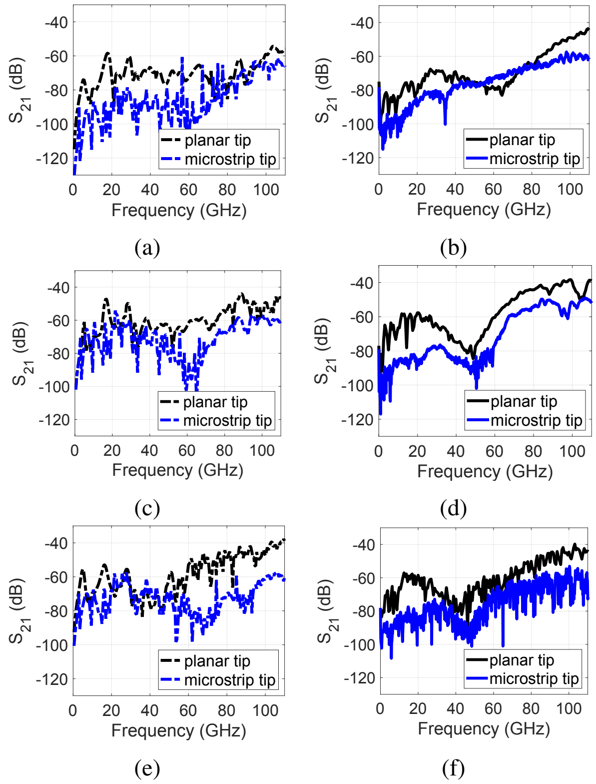

Fig. 3. Coupling between probes for different configurations: (a) simulation and (b) measurement results for probes in the air, (c) simulation and (d) measurement results for substrate on metal chuck, (e) simulation and (f) measurement results for substrate on ceramic chuck.

It is observed that for the probe with planar tips, a parallel plate mode is launched inside the substrate beneath the contact point, becoming stronger with increasing frequency. At 110 GHz, this probe shows an electric field component parallel to the substrate surface. According to the axis definition in Fig. 2a, the TM_0 mode has electric field components in the $\hat{x}$ (E_x) and $\hat{z}$ (E_z) directions, while the TE_1 mode has a component only in the $\hat{y}$ (E_y), all propagating along $\hat{z}$. The excited parallel plate mode at the contact point resembles the E_x component of TM_0, while the surface-parallel electric field aligns with the $\hat{y}$ (E_y) component of TE_1.

Combining insights from Fig. 3d and Fig. 4c, it is concluded that at higher frequencies, especially beyond 55 GHz, the electric field components beneath the contact point couple to surface wave modes with similar field configurations. For the microstrip tip probe, the ground plane shields the signal line from the substrate (Fig. 1b), resulting in a weaker excited parallel plate mode compared to the planar tip probe. Moreover, the electric field at the contact point for the microstrip tip probe shows no significant component parallel to the substrate surface.

For the case where the substrate is located on the ceramic chuck, boundary condition formed by close permittivity of

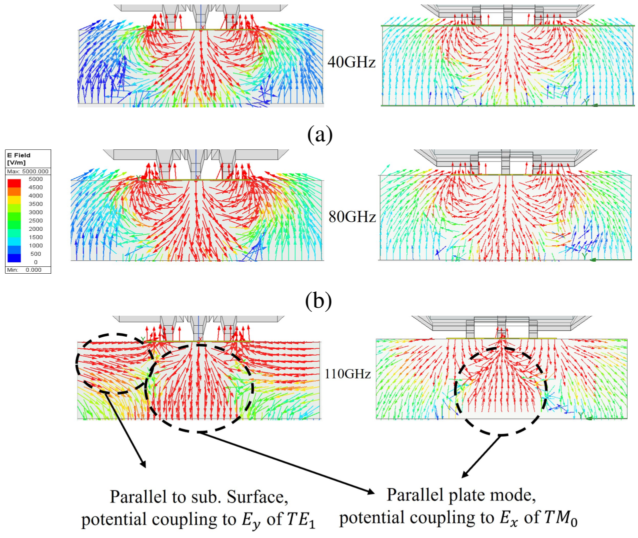

(c)

Fig. 4. Electric field vector distribution at the contact point: planar tip probe (left) and microstrip tip probe (right), with the substrate located on a metallic chuck, at (a)40, (b) 80 and (c) 110 GHz.

alumina and ceramic chuck, and the absence of a metallic surface beneath the substrate, prevent the formation of a parallel plate mode and S_{21} is lower.

To summarize, the contact of the probes with the *THRU*s on the alumina substrate, when located on a metallic chuck, excites a parallel plate mode and an electric field distribution parallel to the substrate around the *THRU*. These fields can in turn couple to TM_0 and TE_1 modes that can propagate within the substrate. For the probe with the planar tip structure, these fields are stronger, leading to stronger modes and stronger coupling (S_{21}) between the probes.

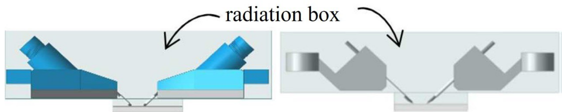

Fig. 5. Studied probe body models with customized radiation box in the simulation setup.

B. *Surface Wave Power Comparison*

This subsection provides further and complementary results by studying the power of surface waves that are generated by the probe contact on the *THRU*s. The calibration substrate is placed on either a metallic or ceramic chuck, with chuck dimensions matching the substrate ($23mm \times 15mm$). Two identical probes are landed on the *THRU*s, spaced 3.7 mm apart, as described previously. A customized radiation box is designed to touch the edges of the substrate and chuck, absorbing waves that reach the edges and suppressing radiation and reflections from them. A graphical illustration of this setup is shown in Fig. 5.

To calculate the power generated by the surface wave, the time-average Poynting vector is calculated on reference sheets of varying heights and located on the four side walls of the radiation box (Fig. 6a). 1 watt of power is injected into the exciter probe port. By summing the power captured on all four sides including the surface which covers the substrate thickness, the total captured power (P_{tot}), which includes both surface wave power (P_{sw}) and air-radiated power (P_{rad}), is determined. To isolate P_{rad} , additional simulations are performed by replacing the portion of the substrate around the *THRU*s with absorbing material with same permittivity as alumina (Fig. 6b), thereby suppressing surface wave propagation inside the substrate. The power captured by the reference sheets in this configuration represents only radiated power from the probe tip and *THRU* contact. P_{sw} is then calculated as $P_{sw} = P_{tot} - P_{rad}$, enabling a clear separation and quantification of surface waves and radiated power contributions.

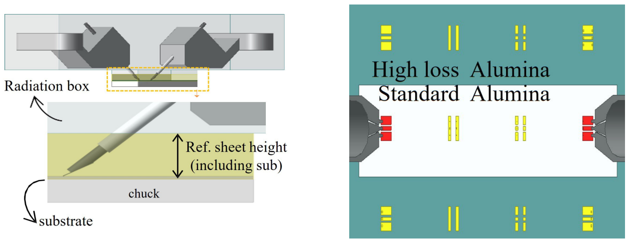

(a) (b)

Fig. 6. Definition of reference sheets for capturing the power at the edges of the substrate, (b) Modification of the substrate to suppress surface waves.

Fig. 7 shows P_{tot} , P_{rad} , and P_{sw} extracted from the simulations, for both probe tip structures for different chuck materials at 90 GHz. It is seen from Fig. 7c that the energy density above the substrate decays exponentially, and P_{sw} reaches a plateau at a reference sheet height of about 1.5 mm. The same trend is observed for the probe with the microstrip tip, but in this case, P_{sw} is about 14 mW lower, highlighting the reduced contribution of this tip geometry to surface wave excitation and radiation compared with the planar tip. For the ceramic chuck, power levels are relatively low, and the total captured power is nearly equal to the radiated power.

To gain insight into the surface wave power level at the frequency where the TE_1 mode is also excited, P_{tot} , P_{rad} , and P_{sw} for the planar tip probe with a metal chuck configuration at 100 GHz are also plotted. As shown in Fig. 7c, at 100 GHz, the surface wave exhibits approximately 10 mW more power compared to 90 GHz.

As we have no direct means to measure P_{sw} in our experimental setup, a different configuration is used in our setup in order to validate simulation results. Two *THRU*s, spaced 3.7 mm apart, are chosen, and two identical probes are landed on the substrate. The second probe, acting as the receiver, is incrementally elevated, and the coupling is measured at each elevation. This setup is shown in Fig. 8.

Fig. 9a–d show the measured coupling for different receiver probe heights. For the probe with the planar tip and the substrate on the metallic chuck, the coupling decreases from

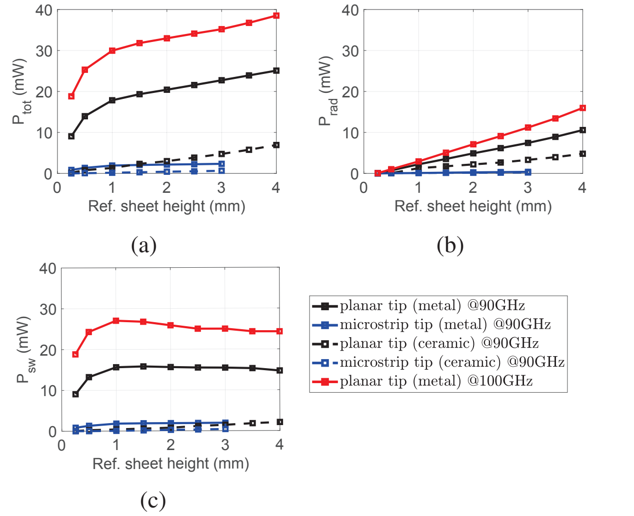

Fig. 7. Simulation results for surface wave power examination at 90 GHz, (a) total captured power, (b) radiated power and, (c) surface power.

the surface up to about 1.5 mm above it for frequencies up to 90 GHz. Around 100 GHz, dips in S_{21} appear due to TE_1 excitation. A similar trend is seen in Fig. 9b for the microstrip tip probe, but with about 10 dB lower coupling than the planar tip probe. Likewise, for the ceramic chuck, the microstrip probe shows an S_{21} about 10 dB lower than the planar tip probe. However, high S_{21} fluctuations and strong radiation contributions complicate analysis for the ceramic chuck. Overall, the measurement agrees with simulations, confirming that the probe contact excites surface waves in the substrate and the power of surface waves is primarily concentrated inside and in the very close vicinity above the substrate, in line with theoretical expectations [10].

As discussed in [4], [5], [11] the excitation of surface waves could significantly impact the quality of the calibration and, consequently, the extraction of electrical parameters during characterization. Additionally, the results reinforce the fact that the probe with the planar tip contributes more to surface wave excitation and radiation into the air, compared with the probe with the microstrip tip.

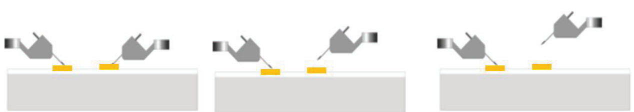

Fig. 8. Configuration of the probes for coupling (S_{21}) measurement at different elevation heights.

III. Conclusion

This study analyzes of how probe tip geometry influences surface wave excitation and radiated power in high-frequency on-wafer measurements, by comparing two commercially available RF probes. It is showed that the probe with planar tip geometry significantly increases surface wave generation, in comparison with the probe with microstrip tip, particularly when the substrate is placed on a metallic chuck, with an estimated surface power level increase of around 14 mW. Such generation of surface waves lead to uncontrolled power distribution in the substrate that is almost impossible to calibrate out and can lead to measurement inaccuracy.

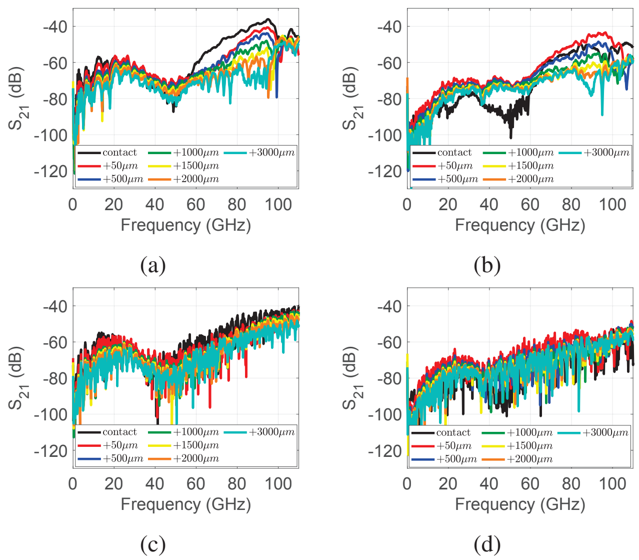

Fig. 9. Configuration of probe for elevation coupling measurement; (a) measured results of the planar tip probe on metal chuck, (b) microstrip tip probe on metal chuck, (c) planar tip probe on ceramic chuck, (d) microstrip tip probe on ceramic chuck.

References

[1] K. Yau, E. Dacquay, I. Sarkas, and S. P. Voinigescu, "Device and IC characterization above 100 GHz," *IEEE Microwave Magazine*, vol. 13, pp. 30–54, Jan. 2012.

[2] A. C. Reniers, A. R. van Dommele, A. B. Smolders, and M. H. Herben, "The influence of the probe connection on mm-wave antenna measurements," *IEEE Transactions on Antennas and Propagation*, vol. 63, pp. 46–58, Jul. 2015.

[3] A. Rumiantsev and R. Doerne, "Rf probe technology: History and selected topics," *IEEE Microwave Magazine*, vol. 14, pp. 46–58, Nov. 2013.

[4] S. Fregonese, M. De Matos, M. Deng, D. Céli, N. Derrier, and T. Zimmer, "Importance of probe choice for extracting figures of merit of advanced mmw transistors," *IEEE Transactions on Electron Devices*, vol. 68, pp. 6007–6014, Oct. 2021.

[5] G. N. Phung, F. J. Schmückle, R. Doerner, *et al.*, "Influence of microwave probes on calibrated on-wafer measurements," *IEEE Transactions on Microwave Theory and Techniques*, vol. 67, pp. 1892–1900, Mar. 2019.

[6] T. Probst, R. Doerner, M. Ohlrogge, R. Lozar, and U. Arz, "110 ghz on-wafer measurement comparison on alumina substrate," in *2017 90th ARFTG Microwave Measurement Symposium (ARFTG)*, Boulder, CO, USA, Nov. 2017, pp. 1–4.

[7] D. Müller, J. Schäfer, D Geenen, *et al.*, "Electromagnetic field simulation of mmics including rf probe tips," in *2017 47th European Microwave Conference (EuMC)*, Nuremberg, Germany, Oct. 2017, pp. 900–903.

[8] E. M. Godshalk, "Surface wave phenomenon in wafer probing environments," in *Proc. 40th ARFTG Conference Digest*, Orlando, FL, USA, Dec. 1992, pp. 10–19.

[9] "Formfactor." (2023), [Online]. Available: https://www.formfactor.com.

[10] D. M. Pozar, *Microwave Engineering: Theory and Techniques*. Hoboken, NJ, USA: John Wiley & Sons, 2021.

[11] C. Yadav, M. Deng, S. Fregonese, *et al.*, "Importance and requirement of frequency band specific rf probes em models in sub-thz and thz measurements up to 500 ghz," *IEEE Transactions on Terahertz Science and Technology*, vol. 10, pp. 558–563, Jun. 2020.